Chapter 1

DNA-Mediated Charge Transport

1.1 Introduction

DNA is canonically known as the repository for genetic information in the cell. Individual strands of DNA consist of a phosphate-deoxyribose backbone connecting nitrogenous bases, either purines (adenine and guanine) or pyrimidines (cytosine and thymine). These individual DNA strands assemble into a right-handed double helical structure according to the hydrogen bonding of the bases: adenine with thymine and guanine with cytosine. The sequence of the nitrogenous bases encodes for proteins according to the central dogma of molecular biology (*1*). Herein, DNA is transcribed into messenger RNA (mRNA), which can then be translated into proteins at the ribosome according to three base codons that correspond to specific amino acids. Chains of amino acids compose proteins, which catalyze important reactions in the cell, such as oxidative phosphorylation to form ATP, the ubiquitous cellular energy currency (*2*).

The nitrogenous bases of DNA are composed of aromatic rings with base-pairs spaced 3.4 Å apart in the double helix (Figure 1). This structure allows the electron density of adjacent bases to overlap, a phenomenon referred to as π-stacking. Significant structural similarity exists between stacked base-pairs in DNA and the z-direction of graphite, a known conductive material. Specifically, the gap between adjacent graphene sheets is 3.354 Å (*3*). The similar spacing of aromatic moieties in graphite and DNA led researchers to hypothesize that DNA could also be conductive.

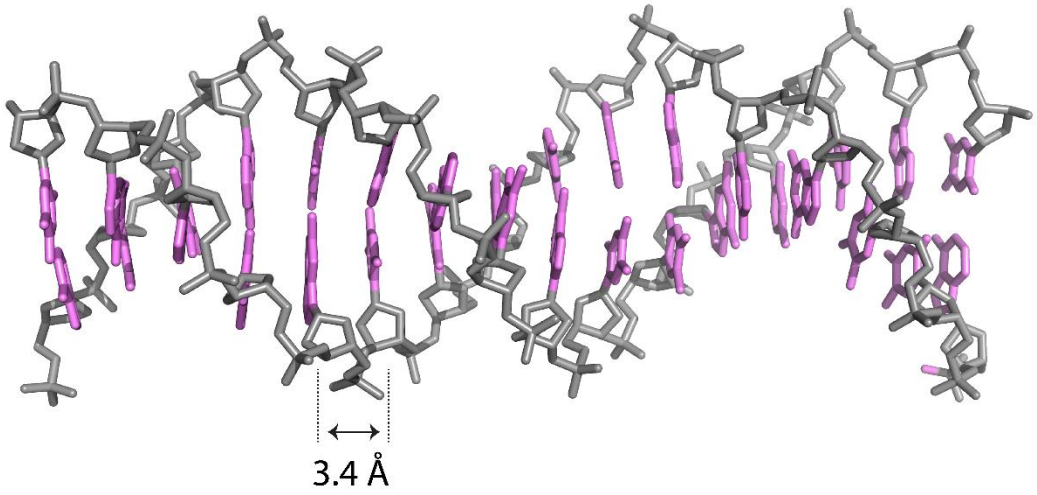

Figure 1. DNA structure with aromatic base-pairs spaced 3.4 Å apart in the double helix. Phosphate-deoxyribose backbone shown in gray, nitrogenous bases in purple. PDB: 3BSE.

1.2 DNA Charge Transport

Decades of research have now established that DNA can indeed conduct charge through the π-stack of the nitrogenous bases in a process termed DNA charge transport (CT) (*4*). Thus in addition to its role as the repository for genetic information, DNA is conductive. Electrons as well as electron holes are efficiently transported through the DNA π-stack (*5*). However, DNA CT is attenuated by disturbances in π-stacking that can occur through DNA mismatches or lesions as well as through protein binding events that significantly bend the DNA (*6-10*). Conversely, nicks in the phosphate-deoxyribose backbone do not impede DNA CT (*11*).

Various platforms for investigating DNA CT have been developed in the Barton group; two of the most effective platforms consist of DNA photooxidant systems in solution (Figure 2), and electrochemistry on DNA monolayers. DNA photooxidants generally contain a planar, aromatic moiety that binds to the DNA via intercalation, wherein the planar photooxidant inserts between two adjacent base-pairs, forming a sandwich-like complex that allows π-stacking between the photooxidant and the DNA bases (*12*). Irradiation of the photooxidant typically produces an excited state that is sufficiently oxidizing and long-lived to withdraw an electron from DNA. Examples of metallointercalators include $[Rh(phi)_2(bpy')]^{3+}$, $[Ru(phen)(bpy')(dppz)]^{2+}$ (which requires a diffusing oxidative quencher to produce a ground state Ru^{3+} oxidant), $[Re(CO)_3(dppz)(py')]^{+}$, and $[Ir(ppy)_2(dppz')]^{+}$, where phi = 9,10-phenanthrenequinone diamine, bpy′ = 4-methyl-4′-(butyric acid)-2,2′-bipyridine, phen = 1,10-phenanthroline,

dppz = dipyrido[2,3-a:2′,3′-c]phenazine, py′ = 3-(pyridin-4-yl)-propanoic acid, ppy = 2-phenylpyridine, and dppz′ = 6-(dipyrido[3,2-a:2′,3′-c]phenazin-11-yl)hex-5-ynoic acid) (*13-15*). The yield of oxidative DNA damage produced by metallointercalators has been found to depend primarily on the thermodynamic driving force for CT, the efficiency of back electron transfer (ET) processes, and the degree of electronic coupling to the DNA π-stack (*15*). These complexes can be covalently tethered to amine-modified DNA via the carboxylic acid moiety appended to either the intercalating (dppz′) or ancillary ligands (bpy′, py′) in order to localize the complex to one end of the DNA (*16*). Organic intercalators such as ethidium and anthraquinone have also been utilized successfully as DNA photooxidants (*13*).

An elegant example of the application of metallointercalators to the study of DNA CT employed intercalating donor $[Ru(phen')(dppz)]^{2+}$ and acceptor $[Rh(phi)_2(phen')]^{3+}$ complexes, where phen′ = 5-amido-glutaric acid-1,10-phenanthroline, covalently tethered to opposite ends of a 15-mer DNA duplex (*17*). $[Ru(phen')_2(dppz)]^{2+}$ is a DNA light-switch complex: whereas its luminescence is quenched in aqueous solution, upon the addition of DNA the ruthenium complex luminesces intensely (*18*). However, when $[Rh(phi)_2(phen')]^{3+}$ is appended to the opposite strand, the DNA-bound $[Ru(phen')_2(dppz)]^{2+}$ luminescence is completely quenched (*17*). Nanosecond time-resolved luminescence experiments were too slow to observe this quenching process. Extensive control experiments, including those that ruled out intermolecular events, coupled with the improbability of energy transfer confirmed that this quenching is due to rapid intramolecular

DNA-mediated electron transfer between the metal complexes, from the $^{*}[Ru(phen')_2(dppz)]^{2+}$ excited state to the rhodium complex.

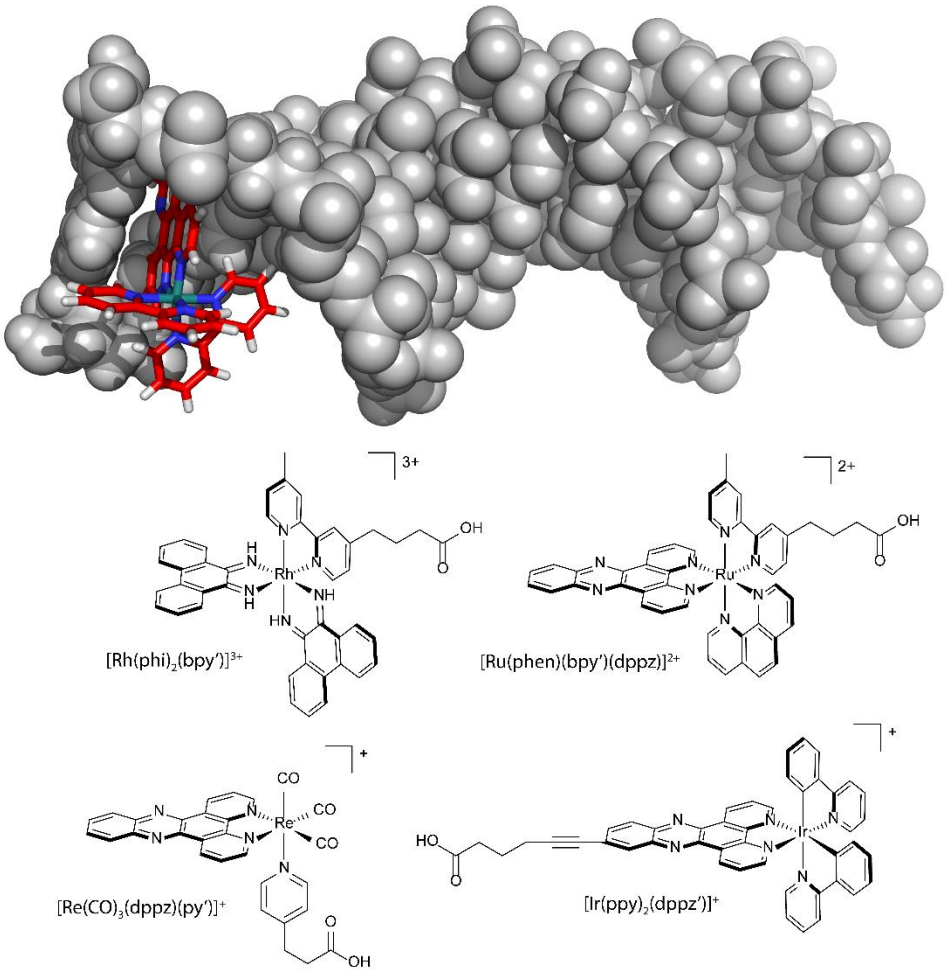

Figure 2. Structures of metallointercalator photooxidants. *Upper*: Crystal structure demonstrating intercalative DNA binding mode with Δ-$[Ru(bpy)_2(dppz)]^{2+}$. Figure created by combining PDB files 3BSE and 4E1U. *Lower*: Examples of commonly used photooxidants: $[Rh(phi)_2(bpy')]^{3+}$, $[Ru(phen)(bpy')(dppz)]^{2+}$ (which requires a diffusing oxidative quencher to produce a ground state Ru^{3+} oxidant), $[Re(CO)_3(dppz)(py')]^{+}$, and $[Ir(ppy)_2(dppz')]^{+}$. Metallointercalators can be tethered to amine-modified DNA via the carboxylic acid moiety appended from the ancillary or intercalating ligand.

1.2.1 Kinetics of DNA CT

Subsequent experiments explored electron transfer between non-covalently bound, intercalated ruthenium and rhodium metal complexes with picosecond spectroscopy (*19*). Even on the picosecond timescale, DNA-mediated charge transport between the metal complexes was faster than the instrumental resolution, with a large decrease in the ruthenium emission intensity at zero time. However, these studies established a lower limit for the electron transfer rate of 3×10^{10} s^{-1} (*19*). Femtosecond transient absorption experiments were finally able to directly observe DNA-mediated electron transfer (*20*). Here, the intercalator ethidium was tethered to one end of the DNA, and the modified base 7-deazaguanine was positioned at varying distances from the ethidium, with either two, three or four intervening base-pairs (10, 14, 17 Å, respectively). Ethidium has a sufficient reduction potential in the excited state (1.2 V versus NHE) to oxidize 7-deazaguanine (1.0 V oxidation potential) but not the other DNA bases, which have higher oxidation potentials. In this study, ethidium was excited using a laser pulse at 500 nm, and a second pulse at 400 nm was used to probe how the absorption of the sample changed as a result of laser excitation (*20*). DNA sequences with guanine substituted for 7-deazaguanine exhibit a lifetime of about 2 ns, corresponding to the inherent rate of decay of the DNA-bound ethidium excited state in the absence of any quenching due to electron transfer. Sequences instead containing 7-deazaguanine show additional 5 ps and 75 ps decay components that can be ascribed to thermodynamically favorable electron transfer from 7-deazaguanine to the ethidium excited state. Fluorescence anisotropy experiments correlated the slower electron

transfer process (75 ps) with the rotation of ethidium in DNA. Therefore, two electron transfer rates were observed that correspond to different ethidium orientations: the 5 ps rate corresponds to an ethidium orientation that is favorable for ET, whereas the slower 75 ps rate corresponds to an initially unfavorable conformation that requires reorientation or rotation of the ethidium in order for ET to occur (*20*). Importantly, the rates of electron transfer are unaffected by donor-acceptor distance from 10 to 17 Å. However, the efficiency of ET was observed to decrease with increasing distance, implicating structural dynamics likely due to the increased probability of transient disorder in stacking, and thus electronic coupling, at longer distances. Overall, this study demonstrated the ultrafast nature of favorable electron transfer through DNA, as well as the shallow distance dependence of the ET rate.

1.2.2 Mechanism and characteristics of DNA CT

Further work has elucidated important aspects of the mechanisms involved in DNA charge transport (*21*). Superexchange involves coherent orbital-mediated tunneling along the entire DNA bridge between the donor and acceptor, and displays an exponential dependence of the rate of electron transfer on distance. This substantial distance dependence with a superexchange mechanism is inconsistent with the fast electron transfer rates that have been measured over relatively long molecular distances (*21*). For example, the DNA-mediated electron transfer from excited $[Ru(phen')(dppz)]^{2+}$ to $[Rh(phi)_2(phen')]^{3+}$ occurs over a distance of 41 Å within just 3 nanoseconds (*17*). Instead, an incoherent hopping mechanism, where there is some intermediate state of charge localization on the bridge, is

more likely for charge transport through DNA because of its more shallow linear distance dependence. However, localized hopping on individual bases is difficult to rationalize with a number of experimental observations (*21*). One of the first clues that pointed towards a delocalized hopping mechanism illustrated the importance of base dynamics by uncovering the temperature dependence of electron transfer through DNA (*22*). In transient absorption experiments with the photooxidant base analog 2-aminopurine as the acceptor and guanine as the electron donor, the rate of ET increased with increasing temperature until duplex melting (*22*). These experiments suggest conformational gating to reach a CT-active state that is enhanced by the increased dynamical motions that modulate electronic coupling at higher temperatures. A periodic length dependence has also been observed in DNA CT (*23-25*). The yield of ET through varying lengths of adenine tracts has been measured by use of a photooxidant with N^2-cyclopropylguanosine (^{CP}G); as the resulting ^{CP}G radical cation undergoes rapid ring opening, the yield of decomposition due to ET can be quantified (*23*,*24*). These studies found an oscillatory component to the distance dependent ET yield with a period of 3 to 4 bases. This result was rationalized by an incoherent CT mechanism wherein charge is delocalized over domains of 3 to 4 bases. Thus, CT is facilitated when the length of the sequence is an integer multiple of these domains, and is less favorable when this is not the case. More recent work by Tao and coworkers investigated the resistance of duplexed DNA between two electrodes (*25*). They found that the resistance of the DNA circuit increases linearly with distance, and observed a periodic oscillation with a period of 2 to 3 bases in sequences with stacked GC base-pairs (*25*). Overall, these experiments suggest

a model for the mechanism of DNA CT. Electron transfer through DNA is best described as an incoherent hopping mechanism, consisting of multiple superexchange steps between delocalized (approximately 3 base pair) domains of well-coupled stacked bases. These CT-active domains of stacked bases are created through conformational dynamics of the bases that modulate their electronic coupling. This mechanism also explains why a mismatch or lesion would attenuate DNA CT: it perturbs the formation of these well-coupled 3 base pair delocalized domains.

A characteristic pattern of oxidative DNA damage results when electron holes are injected into the DNA π-stack with a photooxidant complex such as those described above. Guanine is the most easily oxidized of the DNA bases with an oxidation potential of 1.31 V versus NHE compared to adenine, thymine, and cytosine with potentials of 1.42 V, 1.45 V, and 1.50 V, respectively (*26*). The presence of adjacent guanines can further lower the guanine oxidation potential. Molecular orbital calculations revealed that, of all of the combinations of two stacked bases in DNA, GG/CC has the lowest ionization potential with 70% of the highest occupied molecular orbital (HOMO) localized on the 5′-G of the guanine doublet (*27*). The localization of DNA damage was mapped experimentally using a photosensitizer followed by treatment with hot piperidine (*28*). Piperidine cleaves the DNA backbone at sites of oxidative guanine lesions, as well as abasic sites and other chemical modifications (*29*). This study confirmed that guanine doublets and triplets are electron hole sinks within DNA. Work by Barton and coworkers demonstrated that oxidative damage can be generated from a distance via DNA charge transport, and that this damage is

localized to low potential guanine multiplets (*30*,*31*). Here metallointercalating photooxidants were covalently tethered to one end of the DNA duplex, ensuring spatial separation between the photooxidant and the guanine doublet. Both $[Rh(phi)_2(bpy')]^{3+}$, which is competent to directly abstract electrons from DNA when excited at 365 nm (*30*), and $[Ru(phen)(bpy')(Me_2dppz)]^{2+}$ (where Me_2dppz = 9,10-dimethyl-dipyridophenazine), which requires a diffusing oxidative quencher to produce a ground state Ru^{3+} oxidant in a process known as the flash-quench technique (*31*), were investigated. After irradiation and piperidine treatment of radiolabeled DNA, in both cases damage was observed predominantly at the 5′-G of a guanine doublet located approximately 37 Å away from the site of metallointercalation. Because the timescale of DNA CT (picoseconds) is much faster than the formation of permanent oxidative lesions, the injected electron hole can equilibrate along the base-pair π-stack and localize to the low potential guanine doublet. Thus the pattern of oxidative damage to guanine multiplets is a characteristic of damage from a distance via DNA CT.

The formation of guanine radicals using the flash-quench technique has also been directly observed using transient absorption and EPR spectroscopic methods (*32*,*34*). Nanosecond transient absorption experiments investigated Δ-$[Ru(phen)_2(dppz)]^{2+}$ with a variety of diffusing oxidative quenchers: $[Ru(NH_3)_6]^{3+}$, methyl viologen, and $[Co(NH_3)_5Cl]^{2+}$ (*32*). After the "flash" of laser excitation, the $*Ru^{2+}$ excited state is oxidatively "quenched" by these diffusing species to yield an intercalated ground state Ru^{3+} species with a reduction potential of 1.6 V versus NHE (*33*). In the presence of poly(dAdT) DNA, ruthenium

complex, and diffusing quencher, a long-lived transient ascribed to the decay of the Ru^{3+} species is observed (*32*). However, when poly(dG-dC) is substituted for poly(dA-dT), the long-lived Ru^{3+} transient disappears. Instead, the UV-visible absorbance difference spectrum indicates formation of the neutral guanine radical with maxima at 390 and 550 nm; thus, once formed, the guanine radical cation undergoes rapid deprotonation. The kinetics of the Ru^{2+*} emission decay correspond to the rise of the guanine radical transient, indicating a sequential process. In mixed sequence DNA, the neutral guanine radical transient is long-lived, decaying on a millisecond timescale. Additionally, because $[Co(NH_3)_5Cl]^{2+}$ irreversibly labilizes upon reduction, BET events are inhibited and the highest quantum yield of damage is obtained among the different quenchers (*32*). Guanine radical formation via flash-quench has also been directly monitored spectroscopically via EPR (*34*). When anaerobic samples containing $[Ru(phen)_2(dppz)]^{2+}$, $[Co(NH_3)_5Cl]^{2+}$, and either mixed sequence or poly(dG-dC) DNA were measured at room temperature under continuous irradiation, a signal with an isotropic *g*-value of 2.0048 was observed, whereas this signal was not observed with poly(dA-dT) DNA. These experiments laid the foundation for future studies of DNA-mediated protein oxidation initiated by DNA photooxidation.

1.2.3 DNA electrochemistry

In addition to DNA photooxidant systems in solution, the other major platform that has been effectively used to study DNA CT in the Barton group is electrochemistry on DNA monolayers (Figure 3). Typically, a single strand of DNA is modified with a terminal alkanethiol moiety and annealed to its complementary strand. These thiol-modified DNA

duplexes can then be self-assembled into DNA monolayers on gold electrode surfaces, forming covalent gold-thiol bonds (*35*). Monolayers can be assembled in the absence and presence of $MgCl_2$ to create low and high density monolayers, respectively (*36*). More recently, click chemistry methods have been utilized to enable controlled variation in the amount of DNA on the surface, while concurrently producing more evenly spaced monolayers (*37*). Finally, DNA can also be functionalized with pyrene to form DNA monolayers on highly oriented pyrolytic graphite (HOPG), allowing for a wider potential window than gold electrodes (*38*).

After DNA monolayer formation, a DNA-bound redox probe can be exploited to investigate DNA CT on a surface. Here again, stacking of the redox probe with the DNA base-pair π-stack to facilitate electronic coupling is vital (*39*). The intercalated redox probe may also be covalently tethered to the distal end of the DNA relative to the electrode surface; in this case, the nature of the linkage to the DNA is also important (*40*). Long, saturated linkages do not maintain electronic coupling to the DNA π-stack, in contrast to short, unsaturated linkages which preserve this coupling (*40*). Organic dyes such as nile blue and methylene blue have been commonly used as redox probes (*35*,*36*,*41*). In these systems, charge can flow directly from the electrode to the redox probe, or charge can be conducted in a DNA-mediated fashion, flowing from the electrode through the alkane-thiol tether and the DNA π-stack to reach the redox probe. A DNA-mediated mechanism can be demonstrated by comparing well-matched DNA with DNA that contains a mismatch or abasic site; the disruption to the base pair π-stacking attenuates the amount of charge that reaches the redox

probe. The DNA-mediated pathway can be favored by surface passivation with a backfilling agent such as 6-mercaptohexanol, as well as the use of closely packed monolayers and covalently tethered redox probes with short linkages (*36*). Electrochemical charge transport through the DNA π-stack can occur well below the potential of the DNA bases, likely due to charge delocalization (*21*).

Additionally, redox-active DNA-binding proteins may be utilized as redox probes on DNA-modified electrodes. MutY, a 4Fe4S cluster-containing base excision repair (BER) protein, was the first protein to be thus investigated (*42*). Importantly, these studies were able to determine the DNA-bound redox potential of MutY. The observed redox potential of 90 mV versus NHE was assigned to the $[4Fe4S]^{3+/2+}$ couple, and is consistent with potential ranges for high potential iron-sulfur proteins (HiPIPs). The DNA-mediated nature of the electrochemical signal was confirmed through abasic site discrimination. Finally, a MutY mutant, C199H, where one of the ligating cysteine residues of the 4Fe4S cluster was changed to a histidine, was assayed. C199H MutY displayed a redox potential of 65 mV versus NHE, a negative shift relative to the WT protein as expected for histidine ligation (*42*). This mutant experiment confirmed the iron-sulfur cluster as the origin of the observed electrochemical signal. DNA-modified electrodes have proven a valuable tool for investigating DNA-binding redox-active proteins; their application will be further described in the next section.

DNA electrochemistry experiments have directly demonstrated the shallow distance dependence of DNA charge transport (*41*). Multiplexed chips have been developed that

allow for simultaneous investigation of up to four different types of DNA on a single gold surface with four-fold redundancy (*43*). The multiplexed chips are composed of sixteen individually addressable gold electrodes divided into four quadrants. An elegant application of these chips compared DNA charge transport between 17-mer and 100-mer duplexes covalently modified on the distal end with a nile blue redox probe (*41*). When a chip was modified with half well-matched 100-mer duplex, and half that contained a single C:A mismatch, CT was significantly attenuated even over this long distance. Quantified as cathodic cyclic voltammetry peak area, the ratio of well-matched to mismatched surfaces was 2.3 ± 0.4, similar to what had previously been observed with much shorter DNA duplexes. A second chip was modified with well-matched 100-mer, mismatched 100-mer and well-matched 17-mer DNA and ET kinetics were estimated by measuring the scan-rate dependence of the peak splitting (*41*). The extracted ET rates of 25 - 40 s^{-1} were indistinguishable between the 17-mer and 100-mer duplexes, indicating that tunneling through the alkanethiol tether is rate-limiting (consistent with earlier work, *44*) while ET through the DNA π-stack is rapid. This lower limit for ET through a 100-mer DNA duplex allowed for an estimate of β, an exponential decay parameter characteristic of electronic coupling efficiency that describes the decrease in ET rate with increasing distance between donor and acceptor. The estimated β value for DNA was 0.05 $Å^{-1}$, indicating a much shallower distance dependence than that observed in proteins, where β ranges from 0.85 to 1.5 $Å^{-1}$, with an average value of approximately 1.1 $Å^{-1}$ (*45*). Furthermore, the conformation of the 100-mer duplex on the electrode surface was investigated by cutting with a sequence-

specific restriction enzyme (*41*). Comparing 100-mer duplexes with a restriction site to 17-mer duplexes without such site, almost complete attenuation (90% of the cathodic peak area) of the 100-mer electrochemical signal was observed after incubation with the restriction enzyme as the nile blue-modified section is cleaved and released into solution, while the 17-mer electrochemical signal was unaffected. This established the biologically relevant conformation of the 100-mer DNA on the electrode surface. Overall, this DNA electrochemistry experiment directly demonstrated that charge can be efficiently transported through DNA over long molecular distances, at least up to 100 base-pairs or 34 nm.

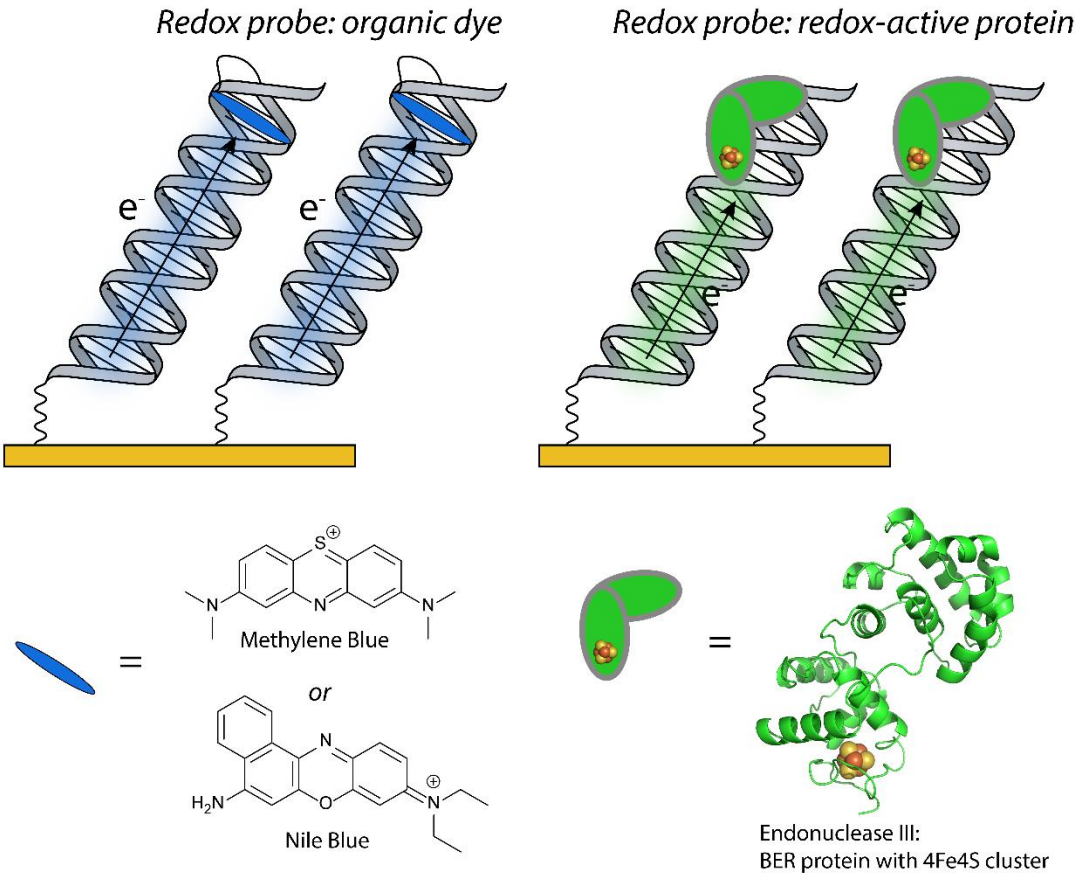

Figure 3. Applications of DNA electrochemistry. DNA monolayers assembled on gold electrodes can be used to probe the ground state DNA-mediated oxidation and reduction of redox probes such as intercalated organic dyes methylene blue or nile blue (*left*) as well as DNA-bound redox active proteins (*right*). Shown is the base excision repair glycosylase Endonuclease III that contains a 4Fe4S cluster. PDB: 2ABK.

1.3 Biological DNA CT

The discovery of the remarkable conductivity of DNA led to speculation about whether DNA CT could be relevant in a biological context inside cells. Because the neutral guanine radical has a relatively long lifetime in DNA (*32*), there is the possibility for interaction with redox-active peptides or proteins that are electronically coupled into the DNA π-stack. This was first demonstrated in proof of principle experiments with the tripeptides KWK and KYK (*46*,*47*), where the aromatic tyrosine (Y) or tryptophan (W) residue intercalates into the π-stack while positively charged lysine (K) residues assist in binding to negatively charged DNA. The oxidation of tyrosine (0.9 V versus NHE) and tryptophan (1.0 V versus NHE) by guanine radical are thermodynamically favorable. Using the flash-quench quench technique with mixed sequence DNA, $[Ru(phen)_2(dppz)]^{2+}$, $[Ru(NH_3)_6]^{3+}$ and KWK, nanosecond transient absorption experiments were used to observe a positive transient at 510 nm that could be assigned to the neutral tryptophan radical given its strong dependence on peptide concentration (*46*). This transient was not present when any of the necessary components (DNA, quencher, or peptide) were omitted. Is this tryptophan oxidation DNA-mediated? First, the peptide itself does not quench the DNA-bound $[Ru(phen)_2(dppz)]^{2+}$ excited state, confirming the absence of direct electron transfer from tryptophan to $*Ru^{2+}$. Given that the free $*Ru^{2+}$ is rapidly quenched (ps) in aqueous solution in the absence of DNA (*18*), further studies compared poly(dA-dT) and poly(dG-dC) DNA. With poly(dG-dC), the rise of the tryptophan radical positive transient at 510 nm corresponds to the disappearance of the guanine radical transient at 373 nm, suggesting

that guanine radical is a necessary intermediate in tryptophan oxidation. In contrast, no positive transient was observed at 510 nm with poly(dA-dT), likely because of fast BET with the diffusing quencher. This control demonstrates that there is no direct contact of KWK with the ground state $[Ru(phen)_2(dppz)]^{3+}$ oxidant. Therefore tryptophan oxidation appears to be mediated by guanine radicals (*46*). Combined with similar experiments using the tripeptide KYK that monitored tyrosine radical formation at 405 nm (*47*), these studies paved the way for work on DNA-mediated protein oxidation.

Indeed, DNA-mediated protein oxidation was soon demonstrated with the methyltransferase HhaI (*48*). This enzyme flips out the central cytosine of its target sequence 5′-GCGC-3′ for methylation, inserting a glutamine side chain (residue 237) into the DNA pocket. Transient absorption experiments with the flash-quench technique utilized a Q237W HhaI mutant, where the intercalating glutamine residue is replaced with aromatic tryptophan. Like studies with the tripeptide KWK, a positive transient corresponding to the neutral tryptophan radical was observed at 510 nm with Q237W HhaI. Here, the ruthenium photooxidant was covalently tethered away from the methylation site, ensuring DNA-mediated tryptophan oxidation. Furthermore, when the distance between the intercalated ruthenium photooxidant and the methylation site is increased from 24 to 51 Å, there was no variation in the rate of transient formation, indicating that CT through the DNA is not rate-limiting (*48*).

1.3.1 Coordination of iron-sulfur cluster DNA processing enzymes via DNA CT

But how could DNA charge transport be used by proteins inside the cell? Following the work with *E. coli* MutY (*42*), other BER proteins with 4Fe4S clusters were discovered to have similar DNA-bound $[4Fe4S]^{3+/2+}$ reduction potentials, including *E. coli* Endonuclease III (EndoIII) and uracil DNA glycosylase (UDG) from *Archeoglobus fulgidus* (*49*). As the first step in the BER pathway, these glycosylase enzymes target and excise specific oxidized lesions within the genome. MutY removes adenine base-paired with 7,8-dihydro-8-oxoguanine (8-oxoG), a result of inaccurate replication of DNA with 8-oxoG, while EndoIII targets oxidized pyrimidines (*50*). After excision of the oxidized or incorrect base to create an abasic site, glycosylase activity is followed by the remaining steps in the BER pathway to restore the integrity of the DNA. While the mechanistic details of glycosylase enzymes once they have found their substrates are relatively well understood (*51*), how the search is efficiently coordinated is less clear given their low copy numbers in the cell. In *E. coli*, there are an estimated 500 copies of EndoIII, and only approximately 30 copies of MutY (*52*). Given their low copy numbers and the vast quantity of DNA that they must search, diffusion-only search models are simply too slow to permit scanning of the entire genome within the doubling time of *E. coli* (*53*).

Could the 4Fe4S cluster of these glycosylase enzymes be involved in the search process? The $[4Fe4S]^{2+}$ cluster of EndoIII is relatively insensitive to reduction and oxidation in solution (*54*), leading to a proposed structural role for the cluster although it is not required for folding or stability in the homologous enzyme MutY (*55*). However, we have

found that the redox potential of the EndoIII cluster shifts upon DNA binding (*56*). The electrochemistry of EndoIII was measured on HOPG electrodes that were either bare or modified with DNA. On DNA-modified HOPG electrodes, the observed midpoint potential of 20 mV versus NHE was assigned to the $[4Fe4S]^{3+/2+}$ couple, similarly to what had been previously reported on DNA-modified gold electrodes. On bare HOPG, two signals were observed: an irreversible anodic peak at 250 mV and a cathodic peak at -300 mV, assigned to the $[4Fe4S]^{3+/2+}$ and $[4Fe4S]^{2+/1+}$ couples, respectively. Thus DNA binding negatively shifts the $[4Fe4S]^{3+/2+}$ redox potential of the cluster by at least 200 mV, activating the cluster towards oxidation (*56*). Because significant conformational changes do not occur upon DNA binding, a thermodynamic consequence of this shift in redox potential is that the oxidized, $[4Fe4S]^{3+}$ form of EndoIII has a much higher affinity for DNA (3 orders of magnitude) than the reduced, $[4Fe4S]^{2+}$ form (*56*). Lower DNA binding affinity for the reduced enzyme was also observed qualitatively with bulk electrolysis experiments on EndoIII, MutY, and UDG (*49*). Therefore while these proteins are relatively insensitive to oxidation in solution, the redox potential of the 4Fe4S cluster shifts into the physiologically relevant range when bound to DNA.

The combination of (*i*) the negative shift in redox potential of the 4Fe4S cluster of glycosylase enzymes upon DNA binding that entails higher binding affinity in the oxidized $[4Fe4S]^{3+}$ state compared to the reduced $[4Fe4S]^{2+}$ state, (*ii*) similar DNA-bound $[4Fe4S]^{3+/2+}$ redox potentials of approximately 80 mV versus NHE for all of the enzymes studied, and (*iii*) the rapid kinetics of DNA CT (ps), suggested a model whereby these proteins could use

interprotein DNA-mediated CT, in a kind of electron transfer self-exchange reaction, to cooperate in order to find lesions inside the cell (*53*) (Figure 4). In this model, a 4Fe4S cluster-containing repair enzyme binding DNA in the reduced form can become oxidized by guanine radicals in the DNA. A second 4Fe4S cluster-containing enzyme can bind within (at a minimum) 100 bases of the first enzyme, becoming activated towards oxidation and releasing an electron into the π-stack of the DNA. This electron can reduce the first distally bound repair enzyme via DNA CT if the intervening DNA is undamaged, resulting in dissociation of this reduced enzyme. Because the DNA-bound redox potentials of the clusters are very similar, this interprotein DNA-mediated CT can be viewed as an activationless self-exchange ET reaction. However, if there is a lesion in the DNA between the proteins, DNA CT will be attenuated and the electron will not reach the distal protein. Instead, both proteins will remain bound to the DNA and can processively diffuse to the location of damage. In this manner, the range over which the slower process of diffusion must occur is significantly reduced. Thus we propose that DNA-mediated signaling would be an efficient way to localize BER proteins to the vicinity of DNA lesions within the cell.

Experiments first focused on gathering *in vitro* evidence for the feasibility of 4Fe4S cluster-protein oxidation by guanine radicals through DNA CT (*57*,*58*). MutY oxidation via the flash-quench technique was monitored by EPR and transient absorption spectroscopies (*57*). With poly(dG-dC) DNA, $[Ru(phen)_2(dppz)]^{2+}$, and diffusing quencher, a mixture of $[4Fe4S]^{3+}$ and its decomposition product, the $[3Fe4S]^{+}$ cluster, is detected upon irradiation in the presence of MutY with low temperature EPR. When poly(dA-dT) is

substituted, a significantly lower intensity EPR signal is observed. With transient absorption and poly(dG-dC) in the absence of protein, a positive transient at 405 nm that decays after approximately 100 μs can be assigned to the guanine radical. Upon the addition of MutY, a very long-lived positive transient is observed at 405 nm that can be fit to obtain coefficients for a fast phase and a slow phase. Absorbance difference spectra plotting coefficients of the fast phase as a function of wavelength correspond to what would be expected for guanine radical, whereas that of the slow phase displayed a maximum at 405 nm, as would be expected for $[4Fe4S]^{3+/2+}$ difference spectra. Therefore this slow phase species can be ascribed to oxidized MutY, likely $[4Fe4S]^{3+}$. The long-lived positive transient is not observed with poly(dA-dT). Furthermore, the yield of guanine oxidation was monitored biochemically in radiolabeled mixed sequence DNA containing a guanine doublet (*57*). In the absence of MutY, damage is localized specifically to the 5′-G of the guanine doublet as expected for oxidative damage generated through DNA CT; this damage is inhibited upon titration of MutY. Overall, these data indicate that while MutY can be oxidized without guanine radical as an intermediate, the thermodynamically favorable oxidation of the MutY $[4Fe4S]^{2+}$ cluster by guanine radical enables more efficient MutY oxidation (*57*). Subsequently, EPR experiments with a nitroxide spin label conjugated to uracil within the DNA sequence demonstrated the feasibility of ET from both EndoIII and MutY to the oxidized spin label (*58*). The EPR-active, $S = ½$ nitroxide species can be oxidized with a mild Ir^{4+} oxidant to yield an EPR-silent species with a reduction potential sufficient to oxidize the $[4Fe4S]^{2+}$ cluster of BER proteins. The reappearance of the nitroxide signal upon the addition of

protein indicates iron-sulfur cluster oxidation to reduce the spin label. A DNA-mediated mechanism is suggested because of the dependence of spin probe reduction on the electronic coupling of the nitroxide spin label: when the spin label is well-coupled to the DNA via an unsaturated linkage, the nitroxide is efficiently reduced, whereas the yield is significantly attenuated with a poorly coupled saturated linkage (*58*).

The iron-sulfur clusters of DNA repair proteins can be oxidized by guanine and modified bases, but could DNA CT be feasible under cellular conditions? In eukaryotic cells, genomic DNA is not freely accessible, but is instead wrapped around histones to form nucleosome core particles. To address the feasibility of DNA CT in nucleosome core particles, Núñez *et al.* investigated oxidative DNA damage induced by covalently tethered $[Rh(phi)_2(bpy')]^{3+}$ in DNA wrapped around histones (*59*). The level of damage to a distal guanine doublet was nearly identical between bare DNA and histone-wrapped DNA, indicating that DNA CT is not attenuated by packaging into nucleosome core particles. Furthermore, there is significant protein traffic on DNA in living cells, including transcription factors and DNA processing enzymes. While DNA CT is attenuated by protein binding events that distort DNA π-stacking by significantly bending the DNA (i.e., TATA binding protein) or flipping out a DNA base, DNA CT is preserved amidst protein traffic that maintains DNA π-stacking (*10,60*). In fact, DNA CT can even be slightly enhanced by protein binding, potentially due to the rigidifying effect of protein binding on base stacking (*60*). Hence DNA CT can occur in nucleosome core particles and is tolerant of most protein traffic, making it feasible *in vivo*.

Subsequent work in the Barton group focused on garnering both *in vitro* and *in vivo* evidence for interprotein signaling via DNA CT. Our model predicts a redistribution of BER proteins from regions of undamaged DNA to the vicinity of a lesion. Using atomic force microscopy (AFM), we have shown that WT EndoIII does indeed redistribute from short well-matched DNA strands onto long strands containing a lesion (*53*). This lesion is a single C:A mismatch which inhibits DNA CT but is not itself a substrate for EndoIII. Redistribution is quantified as a binding density ratio, *r*, of the number of proteins on the long mismatched strands relative to those on short matched strands; a binding density ratio of 1 would indicate equal protein distribution. For WT EndoIII, a binding density ratio of 1.6 ± 0.09 is observed that is even more pronounced in the presence of increasing concentrations of hydrogen peroxide. According to the model, some level of protein oxidation is necessary for redistribution; this is enhanced under conditions that simulate oxidative stress in the cell. Redistribution is also dependent on the proficiency of the protein for DNA CT. Aromatic amino acid residues are known to mediate electron transfer in proteins, accelerating long-distance ET processes that would otherwise be kinetically infeasible (*61*). Y82 in *E. coli* EndoIII is a conserved, aromatic residue in close proximity to the DNA backbone. Mutating this aromatic tyrosine residue to an alanine (Y82A) results in a protein that is electrochemically deficient in DNA CT but proficient in enzymatic glycosylase activity (*53*). Likely because of poorer electronic coupling, less charge can be passed to the iron-sulfur cluster, resulting in a lower signal intensity in cyclic voltammetry experiments. Importantly, Y82A EndoIII is unable to redistribute onto mismatched strands

in the AFM assay because of its inability to perform effective DNA CT. Furthermore Boal *et al.* report an assay measuring the cooperativity of BER proteins *in vivo* (*53*). The "helper function" assay quantifies MutY activity in *E. coli*; thus, a gene of interest can be knocked out to investigate the resultant effects on MutY activity inside living cells. While the details of this assay will not be discussed here, given the strain that is utilized, colonies that are able to grow under specific conditions are "revertants" that result from decreased MutY activity. When the gene for EndoIII is knocked out, MutY activity is decreased even though MutY and EndoIII target different lesions within the cell, indicating that EndoIII contributes to MutY activity by some other mechanism. DNA-mediated signaling between EndoIII and MutY to assist the very low copy number MutY to localize to the vicinity of lesions is suggested by experiments with EndoIII mutants. Restoring CT-deficient Y82A EndoIII does not rescue MutY activity. Conversely, D138A EndoIII, while deficient in glycosylase activity, retains an intact 4Fe4S cluster, and is able to rescue MutY activity. Consequently, the important factor for EndoIII rescuing MutY activity is proficiency for DNA CT. Overall, this helper function assay was the first demonstration of interprotein DNA CT within cells.

Other DNA repair proteins outside the BER pathway have been found with similar DNA-bound $[4Fe4S]^{3+/2+}$ redox potentials. XPD is an ATP-dependent nucleotide excision repair (NER) helicase with a 4Fe4S cluster. On DNA-modified electrode, archaeal XPD from the thermophile *Sulfolobus acidocaldarius* (SaXPD), which shares approximately 22% sequence identity with the human homolog, was found to have a DNA-bound potential of

80 mV versus NHE that is sensitive to an intervening mismatch (*62*). Interestingly, an increase in the electrochemical signal intensity is observed upon the addition of ATP to SaXPD on the DNA-modified electrode surface, but is not observed in the presence of the slowly hydrolyzable analog ATP-γ-S. An ATPase and helicase deficient mutant, G34R XPD, also does not display this increase in current. The signal increase upon ATP addition was ascribed to conformational changes associated with ATP hydrolysis, demonstrating that DNA-mediated electrochemistry can report on enzymatic activity (*62*).

AFM studies combining EndoIII and XPD give direct *in vitro* evidence for interprotein DNA-mediated signaling (*63*). Initial AFM studies showed that WT XPD redistributes from short matched DNA strands to long mismatched strands with a binding density ratio (r = 1.54 ± 0.08) similar to that of WT EndoIII. In contrast, L325V XPD, an electrochemically CT-deficient XPD mutant, does not redistribute analogously to Y82A EndoIII. Equimolar mixtures of XPD and EndoIII were then assayed at concentrations where approximately 2 proteins are bound per DNA strand. Remarkably, mixtures of the *E. coli* BER protein EndoIII and archaeal NER protein XPD efficiently redistribute, localizing to the vicinity of a DNA lesion (*63*). However, this redistribution is not observed if either protein in the mixture is CT-deficient (i.e., WT XPD with Y82A EndoIII, WT EndoIII with L325V XPD, or WT XPD with L325V XPD), likely because at these protein loadings of approximately 2 proteins per strand, a CT-deficient protein results in no partner for the electron self-exchange reaction. When WT XPD is titrated into Y82A EndoIII at a ratio of 3:1, efficient redistribution is recovered because there is a significant population of partners

of CT-proficient proteins. Therefore, given similar DNA-bound redox potentials of their $[4Fe4S]^{3+/2+}$ clusters, proteins from different repair pathways, and even different organisms, can use DNA-mediated CT to cooperate in order to find lesions.

DinG is an *E. coli* DNA damage-inducible helicase with a 4Fe4S cluster and homology to XPD as well as other eukaryotic helicases. DinG performs the vital function of unwinding RNA-DNA hybrid structures, called R-loops, which result from stalled replication forks (*64*). When investigated on DNA-modified electrodes, DinG displays a DNA-bound redox potential of 80 mV versus NHE, the same DNA-bound $[4Fe4S]^{3+/2+}$ potential that had been observed for the BER proteins and SaXPD (*49*,*62*). Like the fellow ATP-dependent helicase XPD, the intensity of the DinG electrochemical signal increases upon the ATP addition. Utilization of the AFM assay demonstrated *in vitro* redistribution with WT DinG only as well as with equimolar mixtures of WT DinG and EndoIII proteins; conversely, redistribution does not occur in a 1:1 mixture of WT DinG with Y82A EndoIII. A modest decrease in MutY activity *in vivo* upon knocking out DinG is observed in the "helper function" assay. This effect can be rescued by complementing with D138A EndoIII but not Y82A EndoIII, suggesting DNA-mediated cross-talk between MutY, DinG, and EndoIII inside cells (*64*).

A much more dramatic *in vivo* result was found with the InvA strain of *E. coli*. By inverting the highly transcribed ribosomal RNA operon, this strain contains an increased frequency of collisions between the transcriptional and replication machinery, forming stalled replication forks (*65*). The resulting RNA-DNA hybrid structures must be unwound

by DinG to maintain cellular viability. Signaling between DinG and EndoIII was investigated *in vivo* by knocking out the gene for EndoIII within the InvA *E. coli* strain. Bacterial growth is severely impaired in this InvA EndoIII knockout strain. An R-loop phenotype was implicated by rescue with RNaseH, as this enzyme selectively degrades RNA in RNA-DNA hybrids. Bacterial growth could also be restored by complementation with WT or D138A EndoIII on a plasmid, but not Y82A EndoIII, implying a DNA CT mechanism (*64*). This is compelling *in vivo* evidence for DNA CT between DinG and EndoIII to assist DinG in maintaining cellular viability under the adverse conditions caused by increased collisions between the transcriptional and replication machinery.

Currently, the number of DNA processing enzymes that contain 4Fe4S clusters continues to increase. For example, in addition to glycosylase and helicase enzymes, 4Fe4S clusters have been found in RNA polymerase (*66*), all four yeast B-family DNA polymerases (*67*), as well as in primase (*68*). As more potential electron self-exchange partners are discovered, DNA-mediated signaling becomes an increasingly viable mechanism to coordinate diverse cellular processes.

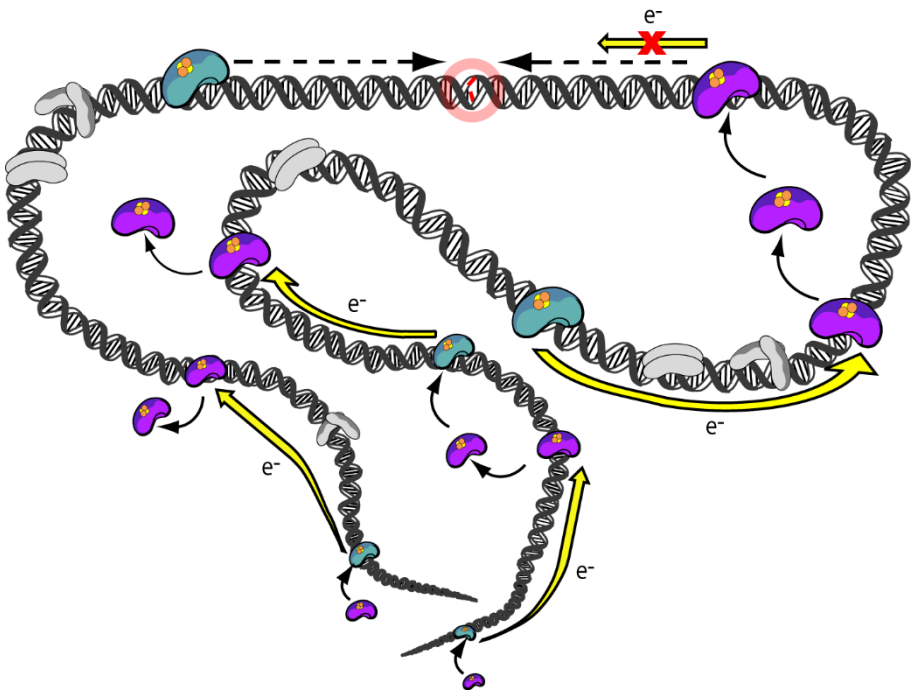

Figure 4. Model whereby 4Fe4S cluster-containing DNA processing enzymes proteins could use interprotein DNA charge transport to cooperate in order to efficiently find lesions inside the cell. This DNA-mediated electron transfer self-exchange reaction depends on similar DNA-bound $[4Fe4S]^{3+/2+}$ reduction potentials and a lower DNA affinity in the reduced, $[4Fe4S]^{2+}$, state compared to the oxidized $[4Fe4S]^{3+}$ state. When the DNA intervening between the two 4Fe4S cluster-containing proteins (shown in purple and teal) is undamaged, the self-exchange reaction can proceed efficiently, with the result that one of the DNA-bound proteins is reduced and its affinity for DNA lowered. This reduced protein can then diffuse to another region of the genome. However, in the case of an intervening mismatch or lesion that disrupts π-stacking and attenuates DNA CT, this self-exchange reaction is inhibited. Both proteins will remain bound to the DNA in the vicinity of the lesion, significantly reducing the range over which the slower process of diffusion must occur. This search process is not interrupted by protein traffic (gray) that does not disrupt DNA π-stacking. Taken from reference 4.

1.3.2 Long-range activation of redox-active transcription factors via DNA CT

DNA charge transport may also be used biologically for the long-range and selective activation of redox-active transcription factors (Figure 5). SoxR is a homodimeric bacterial transcription factor that responds to superoxide stress, containing a $[2Fe2]^{2+/+}$ cluster within each monomer (*69*). In *E. coli*, oxidation of the 2Fe2S cluster of SoxR causes a conformational change which improves an RNA polymerase binding site, stimulating transcription of SoxS, a secondary transcription factor, which in turn induces the transcription of about 100 genes to combat superoxide stress (*70*). Controversy remains regarding the direct oxidant of SoxR *in vivo*. While *in vitro* experiments support direct oxidation of the 2Fe2S cluster by superoxide (*71*), *in vivo* experiments observe weak induction by superoxide and instead suggest SoxR oxidation by redox cycling drugs (*72*) or the modulation of cellular NADPH content (*73*).

Adding to the confusion, the redox potential $[2Fe2]^{2+/+}$ in solution (-290 mV versus NHE) is such that SoxR could be oxidized by many cellular oxidants, even in the absence of oxidative stress. We have found that DNA binding shifts the redox potential of the 2Fe2S cluster of SoxR (*74*). The positive shift in potential by 0.5 V to 200 mV versus NHE upon DNA binding means that DNA-bound SoxR is primarily in its transcriptionally inactive, reduced form *in vivo*. Work by Paul Lee *et al.* then established the viability of SoxR transcriptional activation through long-range DNA-mediated oxidation (*75*). First, it was demonstrated that reduced SoxR with remaining dithionite, but not oxidized SoxR or dithionite alone, inhibits oxidative damage to a guanine doublet that had been generated via

the flash-quench technique. Moreover, SoxR can be activated *in vivo* using the photooxidant $[Rh(phi)_2bpy]^{3+}$, which specifically induces DNA damage rather than general production of reactive oxygen species such as would be expected by redox-cycling drugs. *E. coli* cells were treated with $[Rh(phi)_2bpy]^{3+}$, irradiated, and the resulting level of *soxS* mRNA transcript quantified by reverse transcription PCR (RT-PCR) (*75*). Under these conditions, but not in a dark control that contained Rh but was not irradiated, or a light control that was irradiated but lacked Rh, the *soxS* transcript is significantly induced, indicating the feasibility of SoxR activation by DNA oxidation in cells. Finally, an abortive transcription assay was used to directly observe transcriptional activation from a distance through DNA-mediated oxidation of SoxR. Here, $[Rh(phi)_2(bpy')]^{3+}$ was tethered to the 5′ end of the DNA, 80 base-pairs from the SoxR binding site. The DNA sequence also contained the promoter binding regions of *soxS*, where upon SoxR oxidation, RNA polymerase will bind and initiate *soxS* transcription. Starting with reduced, transcriptionally inactive SoxR, samples were irradiated, and then incubated with RNA polymerase and ribonucleotides. Remarkably, a 4-mer radiolabeled mRNA corresponding to *soxS* could be detected at significant levels. This activation was triggered simply by irradiation that results in DNA oxidation; furthermore, long-distance electron transfer is ensured by the physical separation of the photooxidant and SoxR. These results suggested a model for transcriptional activation of SoxR: reactive oxygen species can abstract electrons from DNA; electron holes thus produced will localize to low potential sites within the DNA, i.e., guanine multiplets; SoxR can then become rapidly oxidized via DNA CT, filling the guanine radical hole and thus becoming

transcriptionally active (*75*). Transcriptional activation from a distance via DNA CT could be a unifying mechanism for SoxR stimulation *in vivo*.

p53 is a tetrameric transcription factor that has vital roles as a tumor suppressor in humans (*76*). p53 decides cellular fates by selective binding to different promoter sites within the genome, for instance, favoring DNA repair and survival or, instead, apoptotic cell death. While p53 does not contain a 4Fe4S cluster, there is a network of redox-active cysteine residues whose oxidation state modulates p53 DNA binding. Specifically, p53 oxidation promotes dissociation from the DNA. Given the close proximity of some of these redox-active cysteine residues to the DNA (*77*) and the demonstrated feasibility of disulfide bond formation from a distance via DNA CT (*78*), Augustyn *et al.* investigated whether p53 could be oxidized in a DNA-mediated fashion (*79*). In constructs with the photooxidant anthraquinone tethered to the DNA distally from the p53 consensus sequence, irradiation induced p53 dissociation in an artificial consensus sequence as measured in gel-shift assays. However, this p53 dissociation was not observed with an intervening C:A mismatch, implying a DNA-mediated process. Intriguingly, in natural p53 consensus sequences, this p53 oxidation via DNA CT is sequence-specific. Promoter sequences for the p21 gene, encoding a protein involved in cell cycle arrest, and that for Gadd45, encoding a protein more involved in DNA repair, were compared using anthraquinone constructs. Dissociation of p53 from the Gadd45 consensus sequence was observed upon irradiation, which would serve to downregulate the gene inside cells, while little dissociation was observed from the p21 sequence (*79*). Under overwhelming conditions of oxidative stress within the cell, genes

encoding proteins stimulating DNA repair, such as Gadd45, would be downregulated in favor of those promoting cell cycle arrest and apoptotic pathways, such as p21. The sequence-specific DNA-mediated oxidation and dissociation of p53 provides a mechanism for how this could occur selectively. Finally, preliminary mass spectrometry studies suggested chemical evidence for p53 oxidation.

Further work by Schaefer and Barton elucidated the important factors for the sequence selectivity of p53 dissociation (*80*). Again using anthraquinone constructs, artificial p53 consensus sequences were created where the guanine content of a purine region within the consensus sequence was successively increased, essentially titrating the oxidation potential. Upon irradiation, a consensus sequence containing AAA displayed the lowest level of p53 dissociation, while a sequence with GGG showed the highest level of dissociation. Natural consensus sequences with similar guanine content behaved in the same way: S100A2 with GGG in its consensus sequence dissociated more upon irradiation than the caspase sequence with AGA. Thus p53 is preferentially dissociated when low potential guanine multiplets are located within the consensus sequence. The relative importance of particular cysteine residues in the DNA-mediated oxidation of p53 was subsequently investigated by serine mutagenesis (*81*). The ability to dissociate from the Gadd45 promoter upon DNA-mediated oxidation was assayed for six cysteine to serine p53 mutants. The C275S and C277S mutations, located nearby the DNA interface, most significantly impaired protein dissociation. Mass spectrometry experiments utilized differential thiol labeling with iodoacetamide to directly observe cysteine oxidation. After irradiation of WT and mutant

p53 with anthraquinone constructs, reduced cysteines are labeled with standard iodoacetamide, while cysteines that were participating in a disulfide bond are labeled with isotopically heavy $^{13}C_2D_2$-iodoacetamide. In the WT protein, there is clearly a shift towards isotopically heaving iodoacetamide labeling in the irradiated anthraquinone samples. Because this is a direct indictor of more disulfide bond formation, this experiment definitively shows p53 oxidation via DNA CT (*81*). The WT protein shows an increase in oxidation upon irradiation for all of the observable cysteine residues: C124, C135, C141, C182, C275, and C277. However, the C275S mutant shows a significantly smaller increase in oxidation upon irradiation. Thus, after an electron hole localizes to low potential guanine sites within the p53 consensus sequence, C275 and nearby C277, close to the DNA interface, seem to form an initial disulfide bond that inhibits DNA binding. Disulfide bond exchange could then occur with nearby cysteines in the protein. Overall, the important molecular mechanisms for DNA-mediated oxidation of p53 have been revealed; this is a compelling way for p53 to selectively dissociate from different consensus sequences within the cell.

As evidenced with p53, proteins that contain redox-active cofactors other than iron-sulfur clusters can yet participate in DNA-mediated processes. Of particular interest is the bacterial ferritin Dps, which protects DNA from oxidative stress and is implicated in bacterial survival and virulence (*82*). Some of these Dps proteins non-specifically bind DNA; could there be a DNA-mediated component to their protection?

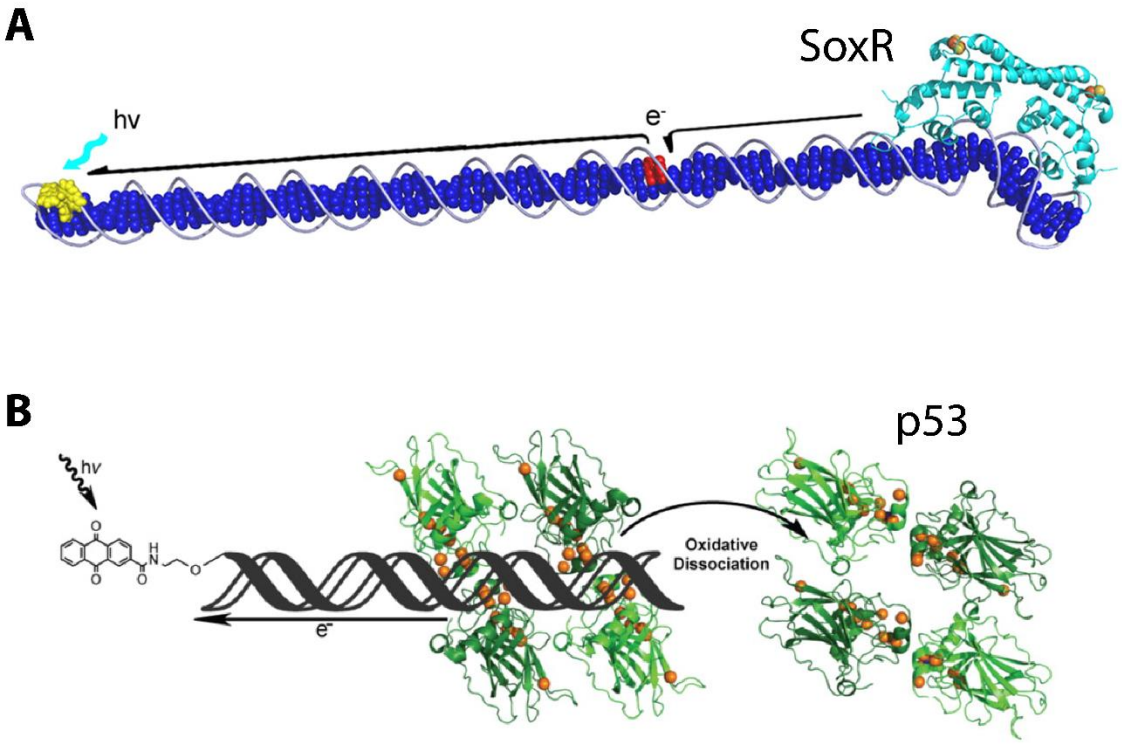

Figure 5. Long-range and selective activation of redox-active transcription factors via DNA charge transport. (*A*) Oxidation and transcriptional activation of the 2Fe2S-cluster containing SoxR, a bacterial superoxide response transcription factor, via long-distance DNA CT to fill guanine radical holes (red). (*B*) Sequence selective oxidation and dissociation of the tumor suppressor p53, which contains a network of redox-active cysteine residues (gold spheres) via DNA CT as a mechanism to decide cellular fates by selective binding to different promoter sites within the genome. Taken from references 75 (copyright © National Academy of Sciences) and 81, respectively.

1.4 Conclusions

DNA charge transport involves the efficient transport of electrons or electron holes through the DNA π-stack over long molecular distances of at least 100 base-pairs. Despite this shallow distance dependence, DNA CT is sensitive to mismatches or lesions that disrupt π stacking and is critically dependent on proper electronic coupling of the donor and acceptor moieties into the base stack. Favorable DNA CT is very rapid, occurring on the picosecond timescale. Because of this speed, electron holes equilibrate along the DNA π-stack, forming a characteristic pattern of DNA damage to low potential guanine multiplets. Furthermore, DNA CT may be used in a biological context. DNA processing enzymes with 4Fe4S clusters can perform DNA-mediated ET self-exchange reactions with other 4Fe4S cluster proteins, even if the proteins are quite dissimilar, as long as the DNA-bound $[4Fe4S]^{3+/2+}$ redox potentials are conserved. For instance, this mechanism would allow low copy number DNA repair proteins to efficiently find their lesions within the cell. DNA CT may also be used biologically for the long-range, selective activation of redox-active transcription factors. The search continues for more proteins that may utilize DNA CT within the cell.

References

1. Lodish, H.; Berk, A.; Zipursky, S.L.; Matsudaira, P.; Baltimore, D.; Darnell, J. *Molecular Cell Biology*, 4th Edition; W. H. Freeman: New York, 2000.

2. Saito, Y.; Yoshikawa, T.; Bandow, S.; Tomita, M.; Hayashi, T. Interlayer spacings in carbon nanotubes. *Phys. Rev. B.* **1993**, *48*, 1907-1909.

3. Chaban, Y.; Boekema E.J.; Dudkina, N.V. Structures of mitochondrial oxidative phosphorylation supercomplexes and mechanisms for their stabilisation. *Biochim. Biophys. Acta* **2014**, *1837*, 418-426.

4. Grodick, M.A.; Muren, N.B.; Barton, J.K. DNA charge transport within the cell. *Biochemistry* **2015**, *54*, 962-973.

5. Elias, B.; Shao, F.; Barton, J.K. Charge migration along the DNA duplex: Hole versus electron transport. *J. Am. Chem. Soc.* **2008**, *130*, 1152-1153.

6. Kelley, S.O.; Holmlin, R.E.; Stemp, E.D.A.; Barton, J.K. Photoinduced electron transfer in ethidium-modified DNA duplexes: Dependence on distance and base stacking. J. Am. Chem. Soc. **1997**, *119*, 9861-9870.

7. Kelley, S.O.; Boon, E.M.; Barton, J.K.; Jackson, N.M; Hill, M.G. Single-base mismatch detection based on charge transduction through DNA. *Nucleic Acids Res.* **1999**, *27*, 4830-4837.

8. Boal, A.K.; Barton, J.K. Electrochemical detection of lesions in DNA. *Bioconjugate Chem.* **2005**, *16*, 312-321.

9. Hall, D.B.; Barton, J.K. Sensitivity of DNA-mediated electron transfer to the intervening π-stack: A probe for the integrity of the DNA base stack. *J. Am. Chem. Soc.* **1997**, *119*, 5045-5046.

10. Gorodetsky, A.A.; Ebrahim, A.; Barton, J.K. Electrical detection of TATA binding protein at DNA-modified microelectrodes. *J. Am. Chem. Soc.* **2008**, *130*, 2924-2925.

11. Liu, T.; Barton, J.K. DNA electrochemistry through the base pairs not the sugar-phosphate backbone. *J. Am. Chem. Soc.* **2005**, *127*, 10160-10161.

12. Li, S.; Cooper, V.R.; Thonhauser, T.; Lundqvist, B.I.; Langreth, D.C. Stacking interactions and DNA intercalation. *J. Phys. Chem. B* **2009**, *113*, 11166-11172.

13. Williams, T.T.; Dohno, C.; Stemp, E.D.A.; Barton, J.K. Effects of the photooxidant on DNA-mediated charge transport. *J. Am. Chem. Soc.* **2004**, *126*, 8148-8158.

14. Shao, F.; Barton, J.K. Long-range electron and hole transport through DNA with tethered cyclometalated Iridium(III) complexes. *J. Am. Chem. Soc.* **2007**, *129*, 14733-14738.

15. Olmon, E.D.O.; Hill, M.G.; Barton, J.K. Using metal complex reduced states to monitor the oxidation of DNA. *Inorg. Chem.* **2011**, *50*, 12034-12044.

16. Holmlin, R.E.; Dandliker, P.J.; Barton, J.K. Synthesis of metallointercalator-DNA conjugates on a solid support. *Bioconjugate Chem.* **1999**, *10*, 1122-1130.

17. Murphy, C.J.; Arkin, M.R.; Jenkins, Y.; Ghatlia, N.D.; Bossmann, S.; Turro, N.J.; Barton, J.K. Long range photoinduced electron transfer through a DNA helix. *Science* **1993**, *262*, 1025-129.

18. Friedman, A.E.; Chambron, J.-C.; Sauvage, J.-P.; Turro, N.J.; Barton, J.K. Molecular "light switch" for DNA $Ru(bpy)_2(dppz)^{2+}$. *J. Am. Chem. Soc.* **1990**, *112*, 4960-4962.

19. Arkin, M.R.; Stemp, E.D.A.; Holmlin, R.E.; Barton, J.K.; Hörmann, A.; Olson, E.J.C.; Barbara, P.F. Rates of DNA-mediated electron transfer between metallointercalators. *Science* **1996**, *273*, 475-480.

20. Wan, C.; Fiebig, T.; Kelley, S.O.; Treadway, C.R.; Barton, J.K.; Zewail, A.H. Femtosecond dynamics of DNA-mediated electron transfer. *Proc. Natl. Acad. Sci. USA* **1999**, *96*, 6014-6019.

21. Genereux, J.C.; Barton, J.K. Mechanisms for DNA charge transport. *Chem. Rev.* **2010**, *110*, 1642-1662.

22. O'Neill, M.A.; Becker, H.-C.; Wan, C.; Barton, J.K.; Zewail, A.H. Ultrafast dynamics in DNA-mediated electron transfer: base gating and the role of temperature. *Angew. Chem. Int. Ed.* **2003**, *42*, 5896-5900.

23. O'Neill, M.A.; Barton, J.K. DNA charge transport: Conformationally gated hopping through stacked domains. *J. Am. Chem. Soc.* **2004**, *126*, 11471-11483.

24. Genereux, J.C.; Augustyn, K.E.; Davis, M.L.; Shao, F.; Barton, J.K. Back-electron transfer suppresses the periodic length dependence of DNA-mediated charge transport across adenine tracts. *J. Am. Chem. Soc.* **2008**, *130*, 15150-15156.

25. Xiang, L.; Palma, J.L.; Bruot, C.; Mujica, V.; Ratner, M.A.; Tao, N. Intermediate tunnelling–hopping regime in DNA charge transport. *Nat. Chem.* **2015**, *7*, 221-226.

26. Fukuzumi, S.; Miyao, H.; Ohkubo, K.; Suenobu, T. Electron-transfer oxidation properties of DNA bases and DNA oligomers. *J. Phys. Chem. A* **2005**, *109*, 3285-3294.

27. Sugiyama, H.; Saito, I. Theoretical studies of GG-specific photocleavage of DNA via electron transfer: Significant lowering of ionization potential and 5′-localization of HOMO of stacked GG bases in B-Form DNA. *J. Am. Chem. Soc.* **1996**, *118*, 7063-7068.

28. Saito, I.; Nakamura, T.; Nakatani, K.; Yoshioka, Y.; Yamaguchi, K.; Sugiyama, H. Mapping of the hot spots for DNA damage by one-electron oxidation: Efficacy of GG doublets and GGG triplets as a trap in long-range hole migration. *J. Am. Chem. Soc.* **1998**, *120*, 12686-12687.

29. Burrows, C. J.; Muller, J. G. Oxidative nucleobase modifications leading to strand scission *Chem. Rev.* **1998**, *98*, 1109-1151.

30. Hall, D.B.; Holmlin, R.E.; Barton, J.K. Oxidative DNA damage through long-range electron transfer. *Nature* **1996**, *382*, 731-735.

31. Arkin, M.R.; Stemp, E.D.A.; Pulver, S.C.; Barton, J.K. Long-range oxidation of guanine by Ru(III) in duplex DNA. *Chem. Biol.* **1997**, *4*, 389-400.

32. Stemp, E.D.A.; Arkin, M.R.; Barton, J.K. Oxidation of guanine in DNA by $Ru(phen)_2(dppz)^{3+}$ using the flash-quench technique. *J. Am. Chem. Soc.* **1997**, *119*, 2921-2925.

33. Delaney, S.; Pascaly, M.; Bhattacharya, P. K.; Han, K.; Barton, J.K. Oxidative damage by ruthenium complexes containing the dipyridophenazine ligand or its derivatives: A focus on intercalation. *Inorg. Chem.* **2002**, *41*, 1966-1974.

34. Schiemann, O.; Turro, N.J.; Barton, J.K. EPR detection of guanine radicals in a DNA duplex under biological conditions: Selective base oxidation by $Ru(phen)_2dppz^{3+}$ using the flash-quench technique. *J. Phys. Chem. B* **2000**, *104*, 7214-7220.

35. Kelley, S.O.; Barton, J.K.; Jackson, N.M.; Hill, M.G. Electrochemistry of methylene blue bound to a DNA-modified electrode. *Bioconjugate Chem.* **1997**, *8*, 31-37.

36. Pheeney, C.G.; Barton, J.K. DNA electrochemistry with tethered methylene blue. *Langmuir* **2012**, *28*, 7063-7070.

37. Furst, A.L.; Hill, M.G.; Barton, J.K. DNA-modified electrodes fabricated using copper-free click chemistry for enhanced protein detection. *Langmuir*, **2013**, *29*, 16141-16149.

38. Gorodetsky, A.A.; Barton, J.K. Electrochemistry using self-assembled DNA monolayers on highly oriented pyrolytic graphite. *Langmuir* **2006**, *22*, 7917-7922.

39. Boon, E.M.; Jackson, N.M.; Wightman, M.D.; Kelley, S.O.; Hill, M.G.; Barton, J.K. Intercalative stacking: A critical feature of DNA charge-transport electrochemistry. *J. Phys. Chem. B* **2003**, *107*, 11805-11812.

40. Gorodetsky, A.A.; Green, O.; Yavin, E.; Barton, J.K. Coupling into the base pair stack is necessary for DNA-mediated electrochemistry. *Bioconjugate Chem.* **2007**, *18*, 1434-1441.

41. Slinker, J.D.; Muren, N.B.; Renfrew, S.E.; Barton, J.K. DNA charge transport over 34 nm. *Nat. Chem.* **2011**, *3*, 228-233.

42. Boon, E.M.; Livingston, A.L.; Chmiel, N.H.; David, S.S.; Barton, J.K. DNA-mediated charge transport for DNA repair. *Proc. Nat. Acad. Sci. USA* **2003**, *100*, 12543-12547.

43. Slinker, J.D.; Muren, N.B.; Gorodetsky, A.A.; Barton, J.K. Multiplexed DNA-modified electrodes. *J. Am. Chem. Soc.*, **2010**, *132*, 2769-2774.

44. Drummond, T. G.; Hill, M.G.; Barton, J.K. Electron transfer rates in DNA films as a function of tether length. *J. Am. Chem. Soc.* **2004**, *126*, 15010-15011.

45. Gray, H.B.; Winkler, J.R. Electron flow through proteins. *Chem Phys Lett.* **2009**, *483*, 1-9.

46. Wagenknecht, H.-A.; Stemp, E.D.A.; Barton, J.K. Evidence of electron transfer from peptides to DNA: Oxidation of DNA-bound tryptophan using the flash-quench technique. *J. Am. Chem. Soc.* **2000**, *122*, 1-7.

47. Wagenknecht, H.-A.; Stemp, E.D.A.; Barton, J.K. DNA-bound peptide radicals generated through DNA-mediated electron transport. *Biochemistry* **2000**, *39*, 5483-5491.

48. Wagenknecht, H.-A.; Rajski, S.R.; Pascaly, M.; Stemp, E.D.A.; Barton, J.K. Direct observation of radical intermediates in protein-dependent DNA charge transport. *J. Am. Chem. Soc.* **2001**, *123*, 4400-4407.

49. Boal, A.K.; Yavin, E.; Lukianova, O.A.; O'Shea, V.L.; David, S.S.; Barton, J.K. DNA-bound redox activity of DNA repair glycosylases containing [4Fe-4S] clusters. *Biochemistry* **2005**, *44*, 8397-8407.

50. Kim, Y.J.; Wilson, D.M. 3rd. Overview of base excision repair biochemistry. *Curr. Mol. Pharmacol.* **2012**, *5*, 3-13.

51. David, S.S.; O'Shea, V.L.; Kundu, S. Base-excision repair of oxidative DNA damage. *Nature*, **2007**, *447*, 941-950.

52. Demple, B.; Harrison, L. Repair of oxidative damage to DNA: Enzymology and biology. *Annu Rev Biochem.* **1994**, *63*, 915-948.

53. Boal, A.K.; Genereux, J.C.; Sontz, P.A.; Gralnick, J.A.; Newman, D.K.; Barton, J.K. Redox signaling between DNA repair proteins for efficient lesion detection *Proc. Natl. Acad. Sci. USA* **2009**, *106*, 15237-15242.

54. Cunningham, R.P., Asahara, H., Bank, J.F., Scholes, C.P., Salerno, J.C., Surerus, K., Münck, E., McCracken, J., Peisach, J., and Emptage, M.H. Endonuclease III is an iron-sulfur protein. *Biochemistry* **1989**, *28*, 4450-4455.

55. Porello, S.L.; Cannon, M.J.; David, S.S. A substrate recognition role for the $[4Fe\text{-}4S]^{2+}$ cluster of the DNA repair glycosylase MutY. *Biochemistry* **1998**, *37*, 6465-6475.

56. Gorodetsky, A.A.; Boal, A.K.; Barton, J.K. Direct electrochemistry of Endonuclease III in the presence and absence of DNA *J. Am. Chem. Soc.* **2006**, *128*, 12082-12083.

57. Yavin, E.; Boal, A.K.; Stemp, E.D.A.; Boon, E.M.; Livingston, A.L.; O'Shea, V.L.; David, S.S.; Barton, J.K. Protein-DNA charge transport: Redox activation of a DNA repair protein by guanine radical. *Proc. Nat. Acad. Sci. USA* **2005**, *102*, 3546-3551.

58. Yavin, E.; Stemp, E.D.A.; O'Shea, V.L.; David, S.S.; Barton, J.K. Electron trap for DNA-bound repair enzymes: A strategy for DNA-mediated signaling. *Proc. Nat. Acad. Sci. USA* **2006**, *103*, 3610-3614.

59. Núñez, M.E.; Noyes, K.T.; Barton, J.K. Oxidative charge transport through DNA in nucleosome core particles. *Chem. Biol.* **2002**, *9*, 403-415.

60. Rajski, S.R.; Barton, J.K. How different DNA-binding proteins affect long-range oxidative damage to DNA. *Biochemistry* **2001**, *40*, 5556-5564.

61. Shih, C.; Museth, A.K.; Abrahamsson, M.; Blanco-Rodriguez, A.M.; Di Bilio, A.J.; Sudhamsu, J.; Crane, B.R.; Ronayne, K.L.; Towrie, M.; Vlček, A. Jr.; Richards, J.H.; Winkler, J.R.; Gray, H.B. Tryptophan-accelerated electron flow through proteins. *Science* **2008**, *320*, 1760-1762.

62. Mui, T.P.; Fuss, J.O.; Ishida, J.P.; Tainer, J.A.; Barton, J.K. ATP-stimulated, DNA-mediated redox signaling by XPD, a DNA repair and transcription helicase. *J. Am. Chem. Soc.* **2011**, *133*, 16378-16381.

63. Sontz, P.A.; Mui, T.P.; Fuss, J.O.; Tainer, J.A.; Barton, J.K. DNA charge transport as a first step in coordinating the detection of lesions by repair proteins. *Proc. Natl. Acad. Sci. USA* **2012***, 109*, 1856-1861.

64. Grodick, M.A.; Segal, H.M.; Zwang, T.J.; Barton, J.K. DNA-mediated signaling by proteins with 4Fe-4S clusters is necessary for genomic integrity. *J. Am. Chem. Soc.* **2014**, *136*, 6470-6478.

65. Boubakri, H.; de Septenville, A.L.; Viguera, E.; Michel, B. The helicases DinG, Rep and UvrD cooperate to promote replication across transcription units *in vivo*. *EMBO J.* **2010**, *29*, 145-157.

66. Hirata, A.; Klein, B.J.; Murakami, K.S. The X-ray crystal structure of RNA polymerase from Archaea. *Nature* **2008**, *451*, 851-854.

67. Netz, D.J.A.; Stith, C.M.; Stümpfeg, M.; Köpf, G.; Vogel, D.; Genau, H.M.; Stodoloa, J.L.; Lill, R.; Burgers, P.M.J.; Pierik, A.J. Eukaryotic DNA polymerases require an iron-sulfur cluster for the formation of active complexes. *Nat. Chem. Biol.* **2011**, *8*, 125-132.

68. Weiner, B.E.; Huang, H.; Dattilo, B.M.; Milges, M.J.; Fanning, E.; Chazin, W.J. An iron-sulfur cluster in the C-terminal domain of the p58 subunit of human DNA primase. *J. Biol. Chem*. **2007**, *46*, 33444–33451.

69. Watanabe, S.; Kita, A.; Kobayashi, K.; Miki, K. Crystal structure of the [2Fe-2S] oxidative-stress sensor SoxR bound to DNA. *Proc. Natl. Acad. Sci. USA* **2008**, *105*, 4121-4126.

70. Imlay, J.A. Cellular defenses against superoxide and hydrogen peroxide. *Annu. Rev. Biochem.* **2008**, 77, 755-776.

71. Fujikawa, M.; Kobayashi, K.; Kozawa, T. Direct oxidation of the [2Fe-2S] cluster in SoxR protein by superoxide. *J. Biol. Chem*. **2012**, *287*, 35702-35708.

72. Gu, M.; Imlay, J.A. The SoxRS response of *Escherichia coli* is directly activated by redox-cycling drugs rather than by superoxide. *Mol. Microbiol.* **2011**, *79*, 1136-1150.

73. Krapp, A.R.; Humbert, M.V.; Carrillo, N. The soxRS response of *Escherichia coli* can be

induced in the absence of oxidative stress and oxygen by modulation of NADPH content. *Microbiology* **2011**, *157*, 957-965.

74. Gorodetsky, A.A.; Dietrich, L.E.P.; Lee, P.E.; Demple, B.; Newman, D.K.; Barton, J.K. DNA binding shifts the redox potential of the transcription factor SoxR. *Proc. Natl. Acad. Sci. USA* **2008**, *105*, 3684-3689.

75. Lee, P.E.; Demple, B.; Barton, J.K. DNA-mediated redox signaling for transcriptional activation of SoxR. *Proc. Natl. Acad. Sci. USA* **2009**, *106*, 13164-13168.

76. Vousden, K.H.; Lu, X. Live or let die: the cell's response to p53. *Nat. Rev. Cancer* **2002**, *2*, 594-604.

77. Cho, Y.; Gorina, S.; Jeffrey, P.D.; Pavletich, N.P. Crystal structure of a p53 tumor suppressor-DNA complex: understanding tumorigenic mutations. *Science* **1994**, *265*, 346-355.

78. Takada T.; Barton, J.K. DNA charge transport leading to disulfide bond formation. *J. Am. Chem. Soc.* **2005**, *127*, 12204-12205.

79. Augustyn, K.E.; Merino, E.J.; Barton, J.K. A role for DNA-mediated charge transport in regulating p53: Oxidation of the DNA-bound protein from a distance. *Proc. Natl. Acad. Sci. USA* **2007**, *104*, 18907-18912.

80. Schaefer, K.N.; Barton, J.K. DNA-mediated oxidation of p53. *Biochemistry* **2014**, *53*, 3467-3475.

81. Schaefer, K.N.; Geil, W.M.; Sweredoski, M.J.; Moradian, A.; Hess, S.; Barton, J.K. Oxidation of p53 through DNA charge transport involves a network of disulfides within the DNA-binding domain. *Biochemistry* **2015**, 54, 932-941.

82. Chiancone, E.; Ceci, P. The multifaceted capacity of Dps proteins to combat bacterial stress conditions: Detoxification of iron and hydrogen peroxide and DNA binding. *Biochim. Biophys. Acta* **2010**, *1800*, 798-805.